Hindawi
Science and Technology of Nuclear Installations
Volume 2020, Article ID 3961095, 14 pages
https://doi.org/10.1155/2020/3961095

Research Article

Nuclear Data Uncertainty Quantification and Propagation for Safety Analysis of Lead-Cooled Fast Reactors

Ishita Trivedi,[1] **Jason Hou**,[1] **Giacomo Grasso**,[2] **Kostadin Ivanov**,[1] **and Fausto Franceschini**[3]

[1]*Department of Nuclear Engineering, North Carolina State University, 2500 Stinson Drive, Burlington Engineering Lab, Raleigh, NC 27695, USA*
[2]*ENEA-FSN-SICNUC-PSSN, v. Martiri di Monte Sole 4, Bologna 40129, Italy*
[3]*Westinghouse Mangiarotti SPA, v. Timavo 59, Monfalcone 34074, Italy*

Correspondence should be addressed to Ishita Trivedi; itrived@ncsu.edu

Received 27 December 2019; Accepted 6 June 2020; Published 12 August 2020

Academic Editor: Arkady Serikov

In this study, the Best Estimate Plus Uncertainty (BEPU) approach is developed for the systematic quantification and propagation of uncertainties in the modelling and simulation of lead-cooled fast reactors (LFRs) and applied to the demonstration LFR (DLFR) initially investigated by Westinghouse. The impact of nuclear data uncertainties based on ENDF/B-VII.0 covariances is quantified on lattice level using the generalized perturbation theory implemented with the Monte Carlo code Serpent and the deterministic code PERSENT of the Argonne Reactor Computational (ARC) suite. The quantities of interest are the main eigenvalue and selected reactivity coefficients such as Doppler, radial expansion, and fuel/clad/coolant density coefficients. These uncertainties are then propagated through safety analysis, carried out using the MiniSAS code, following the stochastic sampling approach in DAKOTA. An unprotected transient overpower (UTOP) scenario is considered to assess the effect of input uncertainties on safety parameters such as peak fuel and clad temperatures. It is found that in steady state, the multiplication factor shows the most sensitivity to perturbations in ^{235}U fission, ^{235}U ν, and ^{238}U capture cross sections. The uncertainties of ^{239}Pu and ^{238}U capture cross sections become more significant as the fuel is irradiated. The covariance of various reactivity feedback coefficients is constructed by tracing back to common uncertainty contributors (i.e., nuclide-reaction pairs), including ^{238}U inelastic, ^{238}U capture, and ^{239}Pu capture cross sections. It is also observed that nuclear data uncertainty propagates to uncertainty on peak clad and fuel temperatures of 28.5 K and 70.0 K, respectively. Such uncertainties do not impose per se threat to the integrity of the fuel rod; however, they sum to other sources of uncertainties in verifying the compliance of the assumed safety margins, suggesting the developed BEPU method necessary to provide one of the required insights on the impact of uncertainties on core safety characteristics.

1. Introduction

In the past two decades, a renewed interest has surfaced in Generation IV lead/lead-bismuth cooled fast reactors (LFRs). Enhanced safety characteristics of lead/lead-bismuth—including relative chemical inertness, retention of hazardous radionuclides such as iodine and caesium, and high boiling point [1]—promote the choice of the LFR as an economically competitive Generation IV reactor with enhanced safety and sustainability. However, LFRs lack of plant operational history, compared to conventional Light Water Reactor (LWR) designs. Insufficient experimental data challenges the trustworthiness of numerical results and therefore accentuates the need for input uncertainty analysis in modelling. Evaluation of these uncertainties provides a better understanding of their impact on the reactor core design and identification of design safety limits.

In this work, the Best Estimate Plus Uncertainty (BEPU) method [2] is used to quantify the impact of nuclear data uncertainties on the performance and safety parameters of LFR systems. In the previous studies, the Total Monte Carlo (TMC) approach assessed the effect of uncertainties originating from lead and plutonium isotopes cross sections on core parameters including criticality and coolant void worth. A comparison of

uncertainties originating from different nuclear data libraries was also provided [3–5]. However, the objective here is to develop a systematic approach for the quantification of nuclear data input uncertainties in LFR systems. Nuclear data uncertainties from ENDF/B-VII.0 cross section libraries are propagated through multiple scales of reactor modelling including lattice, full core, and system level. Sensitivity and uncertainty analysis is performed using generalized perturbation theory (GPT) [6] with variance covariance library COMMARA-2.0 [7]. The analysis also ranks the most contributing nuclide-reaction pairs to total uncertainty of output parameters. The targeted output uncertainties include eigenvalue and reactivity feedback coefficients such as Doppler, core radial expansion, and fuel/coolant/structure density worth coefficients. Nuclear data uncertainties are then propagated through the system model as standard deviations associated with respective feedback coefficients, which are perturbed using stochastic sampling approach to assess core safety capabilities.

2. Reactor Design and Simulation

2.1. Core Description. The demonstration lead-cooled fast reactor (DLFR) core was conceptualized by the Westinghouse Electric Company (WEC) in collaboration with Italian National Agency for New Technologies, Energy and Sustainable Economic Development (ENEA) and Argonne National Lab (ANL). A generic version of the DLFR design is developed and applied to the current study.

The DLFR is a pool-type LFR with the thermal output of 500 MW fuelled with uranium oxide (UO_2). Figures 1 and 2 show one-third of the DLFR core map and the assembly radial layout of the DFLR core, respectively [8]. The core comprises 163 hexagonal assemblies arranged in a triangular lattice with a pitch of 30.4 cm. This includes 82 fuel assemblies divided into two enrichment zones (inner and outer cores) and three safety assemblies, surrounded by 78 reflector/shield assemblies [8].

Finger absorber rods (FARs), as shown in Figure 2, represent unitary elements of regulation, control, and safety banks. Control safety banks are primarily for reactor control whereas regulation rods are utilized for the fine-tuning of reactivity [8]. They are designed to enter the hollow space of a central beam tube in subassemblies (Figure 2(a)) from the top or bottom of the core. Bottom-inserted FARs encapsulate a reflector column atop an absorber column. After a bottom-inserted FAR is withdrawn, the reflector part of the FAR sits beside the active core and the absorber part is located below the core. The top-inserted FARs only have an absorber column. After a top-inserted FAR is withdrawn, the absorber sits above the core, as shown in Figure 2(b) [8].

Three safety assemblies (S2) located in the inner core ring three (Figure 1) are envisioned for SCRAM. Figure 2(b) shows the withdrawn position of S2 assemblies aside a fuel assembly for understanding purposes only.

2.2. Computational Tools and Methodologies. The DLFR core is modelled using the Argonne Reactor Computation (ARC) Code suite, developed, and maintained by ANL [9]. Within ARC, MCC-3.1 [10] coupled with the two-dimensional (2D)

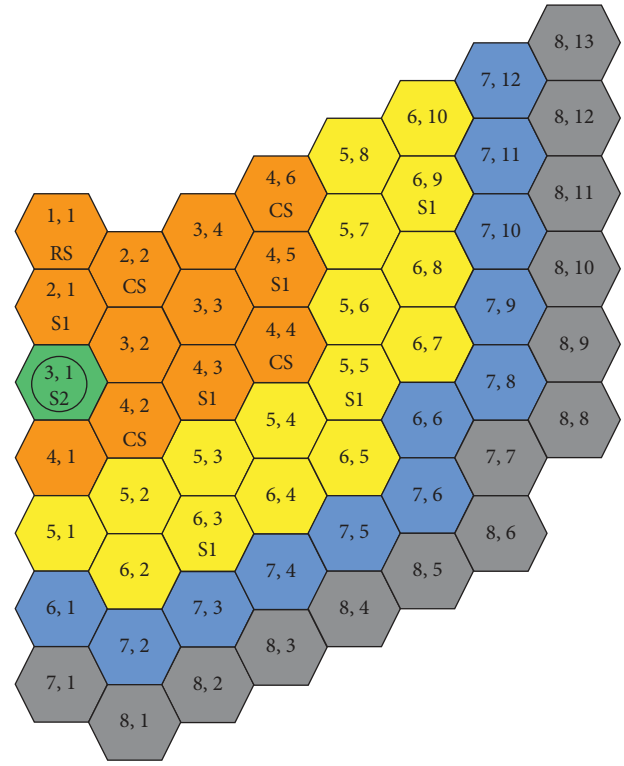

Figure 1: Radial core map with regulation (RS), control (CS), and safety (S1, S2) systems. There are inner and outer core (rings 1–6), reflector (ring 7), and shield (ring 8) subassemblies.

S_N transport solver TWODANT [11] is used to generate the condensed multigroup cross sections. In the conventional method shown in Figure 3, MCC-3.1 first calculates condensed regionwise self-shielded cross sections in 230 ultrafine group (UFG) starting from a 2082-groups ENDF/B-VII.0 master library and provides them to TWODANT [10, 11]. TWODANT performs transport calculations on an equivalent *R-Z* model of the core to derive regionwise flux solutions [11]. In the final step, MCC-3.1 generates regionwise 33 Broad-Group (BG) cross sections using the flux solutions from TWODANT. The DIF3D code receives the cross sections for flux calculations on the whole core using the variational nodal transport solver (VARIANT) [12]. The angular flux solution and scattering approximation are expanded to the 3rd order.

The two-dimensional (2D) assembly and core models are also developed in Serpent 2 [13] for lattice calculations and model verification. Periodic boundary conditions are set on the lattice level. The simulations are performed in the all-rods-out condition with the safety rods (S2) withdrawn below core. Neutron population is set to be 100,000 with 2000 active and 300 inactive neutron generations.

The three-dimensional (3D) model setup maintains an axial temperature gradient for all core components above, below, and at the active core level [8]. Consequently, the neutronics model accounts for temperature dilatation effects on all structural components and material densities. All dimensions and densities are adjusted by factors governed by their respective coefficients of linear thermal expansion:

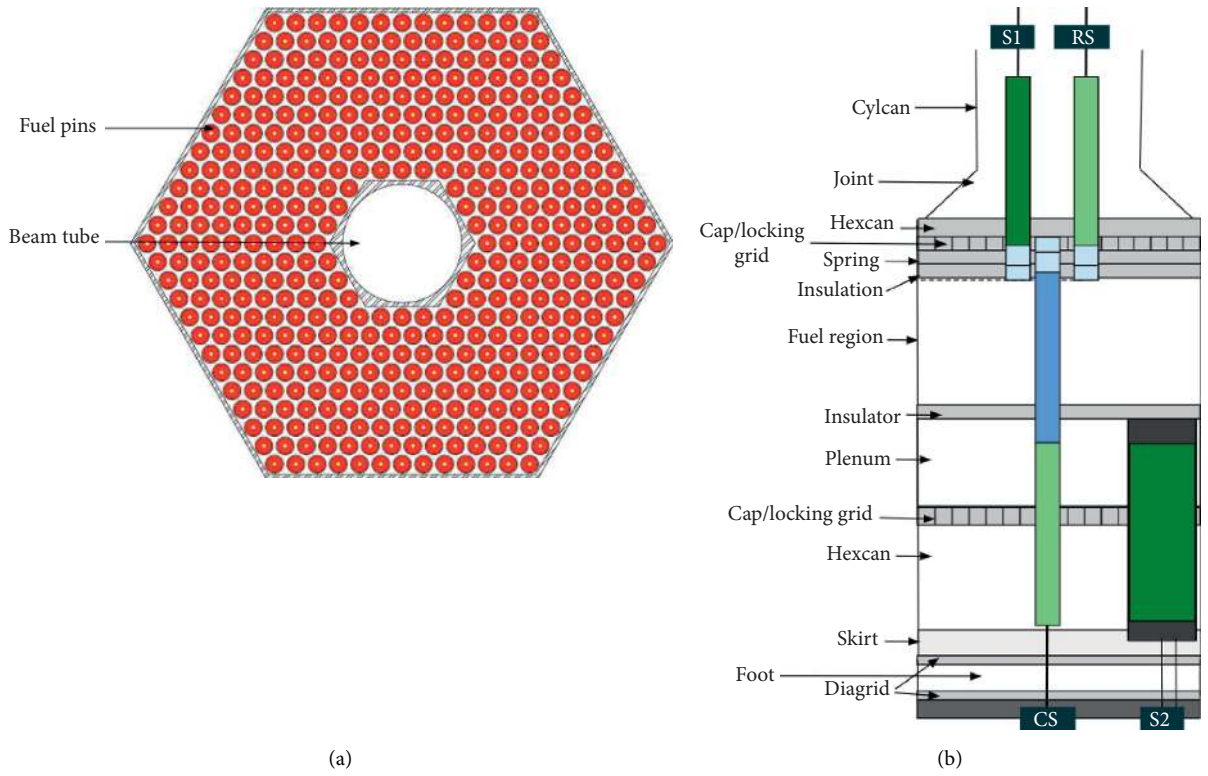

Figure 2: Radial fuel assembly map (a) with axial positioning of regulation (RS), control (CS), and safety (S1, S2) systems in withdrawn position (b).

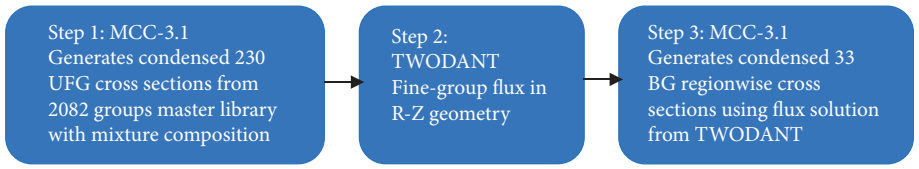

Figure 3: Conventional cross section generation method in ARC.

$$\alpha_T = \frac{1}{L}\left(\frac{dL}{dT}\right), \tag{1}$$

where L and T represent nominal length and expansion temperature, respectively. The thermal expansion data of fuel, coolant, and structural materials are provided in [14, 15].

2.3. Improved Cross Section Generation Method. As detailed previously, the unique design of the DLFR involves partially inserted FARs in the withdrawn position (Figure 2(b)), where the absorber/reflector material sits in the centre of the fuel assemblies. The axial heterogeneity must be preserved for a proper treatment of the self-shielding effects during the cross section generation. Therefore, intermediate steps were developed for improving the accuracy of the self-shielded cross sections in addition to the conventional method shown in Figure 3 where assemblies are homogenized using a zero-dimensional (0D) mixture geometry. The workflow of the improved cross section generation method is given below.

(i) Using the conventional method (Figure 3), DLFR fuel subassembly is represented with various 0D homogenized axial regions, shown in Figure 2(b), in 0D mixture geometry with an equivalent R-Z model in TWODANT. This provides 230-groups region-wise flux solutions in the axial direction for fuel assemblies. MCC-3.1 then computes condensed cross sections in 33 BG for one fuel subassembly type. Such cross sections are generated with the conventional method for each fuel subassembly type individually. Six fuel subassembly types constitute the DLFR—inner core assembly without FAR, inner core assemblies with RS, S1, and CS type FARs, outer core assembly without FAR, and outer core assemblies with S1 type FARs [8].

(ii) Cross sections for nonmultiplying assemblies (shield, reflectors, and S2 safety system) are generated using the conventional process outlined in Figure 3. The core is built with homogenized mixture geometry for different subassemblies

represented with an RZ model (Figure 4) in TWODANT for leakage calculations. Regionwise flux solutions from TWODANT are stored in an *rzmflx* file [11].

(iii) Radial leakage is incorporated in the fuel cross sections from step I. MCC-3.1 performs a separate set of calculations for the active core region utilizing 1D heterogeneous cell treatment capabilities [16]. The 1D cylindrical geometry option of MCC-3.1 is adapted by superimposing *rzmflx* flux spectrum from step II to the 1D cell transport solutions. This approach simultaneously accounts for the heterogeneity effects in the fuel region and interregion leakage effect within the core. Figure 4 shows the 1D fuel assembly model where the beam tube and fuel rings in Figure 2(a) correspond to equivalent cylindrical rings 1, 2, in Figure 5. Each cylinder is now subdivided into 1D subcylinders separating the materials contained within the original cylinder, more details on this methodology are provided in [16].

(iv) Different region cross sections from all subassemblies are merged into one ISOTXS format file for all other calculations.

2.4. Reactor System Model. The reactor system is modelled with the limited, noncommercial version of SAS4A/SASSYS-1, called MiniSAS [17]. MiniSAS excludes some capabilities such as severe accident modelling from SAS4A/SASSYS-1 [18]. The overall system design for DLFR is adapted from the ABR1000 system [19] for preliminary safety analysis due to the unavailability of the actual system model when this work was carried out. The system includes a primary heat transfer system and emergency heat removal system (DRACS) driven by natural circulation. Coolant flows from the hot pool to heat exchangers and returns back into the cold pool. Primary pumps ensure the forced convection of the coolant to extract heat from the reactor. A once-through steam generator is modelled in the secondary circuit. LFR specific parameters are obtained from the existing DLFR data, including a core flow rate of 28,560 kg/s, coolant inlet temperature at 663.3 K, and rated core thermal power of 500 MW [8]. Additional relevant specifications are provided in Table 1.

The reactor core is modelled by two vertical parallel thermal-hydraulic channels, representing the inner core and outer core region, respectively. A single fuel pin structure surrounded by coolant is used for representing each channel. Assembly average power, average coolant flow rate, Doppler feedback coefficient, and axial power profiles are specified individually per channel. The fuel pin is discretized into 10 radial temperature nodes and 20 axial segments [18]. A simple radial expansion model [18] from MiniSAS is incorporated to account for core flowering effect.

2.5. Uncertainty Quantification and Propagation Methods. The Uncertainty Quantification and Propagation (UQ&P) quantifies the influence of input uncertainties on the outputs for a given model. In this section, uncertainties originating from nuclear data are evaluated and propagated through the reactor system to assess their impact on core safety during transients. Deterministic and stochastic sampling methods are considered for UQ&P at different stages of core modelling.

In a large or complex model, with a system of multiple perturbed equations for each input variation, uncertainty analysis via sampling-based methods is not feasible. Nuclear data uncertainty propagation using stochastic sampling is computationally very expensive during cross section generation. An alternative approach is to apply perturbation-based methods for quantifying output uncertainties in the neutronic model. These output parameters are input in the system model where they are stochastically sampled within respective standard deviations. This method will greatly reduce computation time and resources.

As such, generalized perturbation theory (GPT) based on truncating the Taylor expansion of a response parameter [6] is applied to the DLFR core to quantify uncertainties on steady state parameters, namely, the main eigenvalue and reactivity feedback coefficients. Five different feedback coefficients are considered, including the Doppler coefficient, radial expansion coefficient, and fuel/coolant/structure density worth. For Doppler feedback coefficient, fuel temperature is increased by 500 K from the operating temperature (1200 K). The radial expansion is realized by increasing the assembly pitch by 2.5% while preserving the mass of fuel and structure. Fuel, coolant, and structure density worth are computed by introducing a 5% decrease in nominal density in active core region only. These perturbations are chosen based on literature review [20].

Feedback uncertainties are propagated deterministically through the reactor system, while the stochastic sampling method is used to sample input uncertainties and statistically analyse output responses during transients. Both methods and their applications are explained in further sections.

2.6. Generalized Perturbation Theory. GPT uses deterministic sensitivity and uncertainty (S&U) methods to compute sensitivity coefficients. Sensitivity coefficients reflect the relative change of an integral core parameter (such as eigenvalue) with respect to the relative changes in multigroup nuclear data. After obtaining the sensitivities (S_i) associated with each integral parameter, the total contribution of uncertainties attributed to these coefficients can be determined using Pearson correlation coefficients and covariance matrices [6].

For a given core parameter R_i, the sensitivity coefficient matrix $\overrightarrow{S_R}$ is defined as

$$S_R = \begin{bmatrix} S_1 \\ \vdots \\ S_i \\ \vdots \\ S_N \end{bmatrix}, \quad \text{for } 1 \le i \le N, \tag{2}$$

where N is equal to the nuclide-reaction number × energy groups. For example, for ^{235}U fission reaction for 33 energy groups, $N = 1 \times 33$. A sensitivity coefficient relative to an isotope j, a reaction x in an energy group g, is

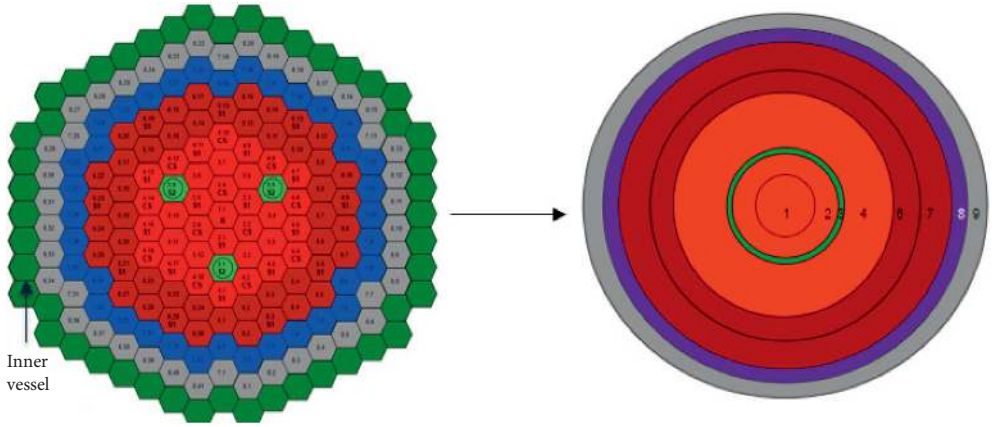

Figure 4: Full core RZ representation in TWODANT.

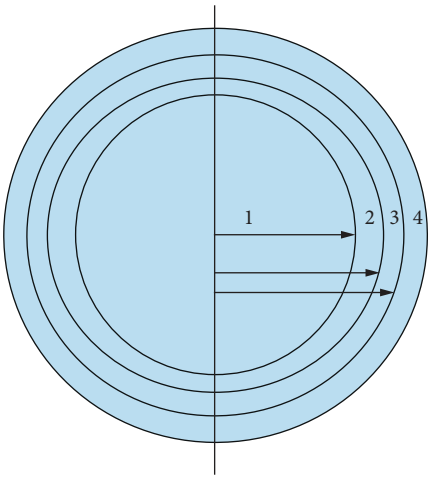

Figure 5: 1D cylindrical representation of the active region in MCC-3.1.

Table 1: System model specifications for the current DLFR system in MiniSAS.

System Components	Description
Coolant flow rate	28,560 kg/s
Coolant inlet	663.3 K
Fuel/coolant type	Oxide/lead
Core channels	2 channels: IC and OC
Heat exchanger (HX)	4 identical HX—1 is modelled in SAS
Steam generator	Once-through SG
Pump	Normalized pump head vs. time provided for the intermediate and primary pumps
Direct reactor auxiliary cooling system (DRACS)	Emergency cooling system

$$S_{j,x,g} = \frac{\partial R/R}{\partial \sigma_{j,x,g}/\sigma_{j,x,g}} = \frac{\partial R}{\partial \sigma_{j,x,g}} \frac{\sigma_{j,x,g}}{R}, \tag{3}$$

with a first-order perturbation, the Sandwich rule derives the uncertainty I_i^2 for the i^{th} core parameter R_i [6, 21] by folding the respective sensitivities with the variance covariance matrix (VCM) of input parameter:

$$I_i^2 = S_i^T D S_i, \tag{4}$$

where D is the variance covariance matrix structured as

$$D = \left(D_{x,j}\right) = \begin{bmatrix} D_{11} & D_{12} & \cdots & \cdots & D_{1N} \\ D_{21} & \cdots & & & \\ \vdots & & D_{jj} & & \\ \vdots & & & \cdots & \\ D_{N1} & & & & D_{NN} \end{bmatrix}. \tag{5}$$

In this work, ENDF/B-VII.0 nuclear data uncertainties provided in 33 energy macrogroups are considered with VCM COMMARA-2.0 [7, 21]. Working versions of COMMARA-2.0 were released and tested by ANL and Idaho National Lab (INL).

Sensitivity ($S_{\alpha,\sigma}$) of a feedback coefficient (α) equation (6) points to changes induced in reactivity from perturbation in nuclear data (σ) as

$$S^{j}_{\rho,\sigma} = \frac{\partial \rho_j}{\partial \sigma_{i,x,g}} \frac{\partial \sigma_{i,x,g}}{\rho_j}, \tag{6}$$

where $j = (1, 2)$ corresponds to a base case and perturbed case, respectively.

The feedback coefficient α is obtained from PERSENT [22]. It represents a change in reactivity between the base and perturbed core states caused by a change in core parameters (temperature/density/pitch). For the Doppler coefficient, a base case sensitivity of reactivity ($S^{1}_{\rho,\sigma}$) to nuclear data perturbations is obtained at nominal temperature. Similarly, a perturbed case provides sensitivities ($S^{2}_{\rho,\sigma}$) at Doppler temperature to perturbations to σ. Then, (7) [13] provides the sensitivity of the feedback coefficient $S_{\alpha,\sigma}$ by combining $S^{1}_{\rho,\sigma}$ and $S^{2}_{\rho,\sigma}$ using the reactivity change ($\Delta\rho = 1/k^1 - 1/k^2$) from the base to the perturbed case [23]:

$$S_{\alpha,\sigma} = \frac{S^{2}_{\rho_2,\sigma}/k^2 - S^{1}_{\rho_1,\sigma}/k^1}{\Delta\rho}. \tag{7}$$

The total uncertainty I^2 of α can be described using (6) as $I^2 = S^{T}_{\alpha,\sigma}\, D\, S_{\alpha,\sigma}$.

PERSENT employs an adjoint-based sensitivity analysis method. Sensitivity functions are evaluated from adjoint variables without solving the system of perturbed equations for each input parameter change. The solution of the corresponding adjoint transport equation includes the change in eigenvalue based on perturbations in cross sections [22]. In Serpent, a collision-history approach computes the GPT calculations, which determines the sensitivity coefficient calculations based on classical perturbation theory [24].

2.7. Stochastic Sampling. The Uncertainty Quantification (UQ) and optimization code DAKOTA [25] extend the uncertainty propagation through transient scenarios using stochastic sampling. DAKOTA is a multilevel parallel object-oriented framework for S&U analysis along with other capabilities [25]. Two types of stochastic sampling-based approaches are available in the DAKOTA—Monte Carlo (MC) and Latin Hypercube Sampling (LHS) method. The LHS approach stratifies each uncertain parameter domain into N bins (N being the number of samples). So, each bin can only contain one sample at a time. Consequently, this method requires fewer samples for convergence than an MC approach, where the samples are randomly selected from the parameter domain [25].

For transient simulations, a Python interface couples DAKOTA to the external code (SAS4A/SASSYS-1) [19]. The coupling was developed at ANL for UQ in Sodium Fast Reactors (SFRs) [19]. DAKOTA drives the interface through a system call, reads the perturbed parameters in the SAS4A/SASSYS-1 input file, and executes the external code to run simulations. A Python script parses the output files to gather responses of interest in "results" file [19]. DAKOTA then reads the "results" file to perform the statistical analysis. The mean and 5%/95% intervals of response functions (peak fuel/clad/coolant temperatures) to 1% perturbation of DLFR feedback coefficients have been studied in this work. Figure 6 provides a schematic understanding of the DAKOTA/SAS4A/SASSYS-1 coupling scheme.

3. Results and Discussion

3.1. Model Verification. Lattice level results from ARC and Serpent are compared to quantify the difference between the models using nominal cases developed at equilibrium core composition. Table 2 provides eigenvalues obtained from an outer core fuel assembly and 2D core at Beginning/End of Cycle (BOC/EOC, resp.). Observed differences in eigenvalues from heterogeneous Monte Carlo and homogenized MCC-3.1/DIF3D calculations are attributed to differences in cross section generation and modelling capabilities of the two codes [10, 13]. A comparison of BOC core power distribution and assembly flux is shown in Figures 7 and 8, which show the relative error is less than 10% for most assemblies. The Monte Carlo relative statistical error from Serpent for all flux and power values is in the order of 10^{-3}. The assemblies showing larger differences of 11.6%, 13.4%, 14.8%, and 16.1% are located in the outer core near reflectors which cause flux distortions in that region.

To quantify the differences from the improved cross section generation methodology, two sets of cross sections are generated using methods outlined in Figures 3 and 9, respectively, for the same core model in DIF3D. A difference of 950 pcm is found at BOC between respective eigenvalues. The new cross section generation method gives k_{eff} of 1.0332 at BOC. The conventional method provides a lower eigenvalue of 1.0231 due to homogenization of fuel and absorber within the assembly. Considering the importance of the self-shielding process, the improved cross section generation approach is adapted for assessing all core performance parameters. Further work is underway to verify these results using code-to-code comparison with Serpent (Monte Carlo). Homogeneous and heterogeneous 2D assembly and core models developed in ARC using the conventional two-step (Figure 3) and improved cross section Figure 9 methods will be compared with the same models developed in Serpent. It is anticipated that the largest difference is from homogenization of absorber regions within the assembly.

3.2. Uncertainty Analysis. This section provides nuclear data UQ results at multiple scales of reactor modelling using a systematic approach. Uncertainties are obtained for steady state parameters including eigenvalue and feedback coefficients using statistical correlations from COMMARA-2.0. Top nuclide-reaction pair uncertainty contributors to respective parameters are also identified. Uncertainties are further propagated to the system model for computing standard deviations of fuel/clad/coolant temperatures

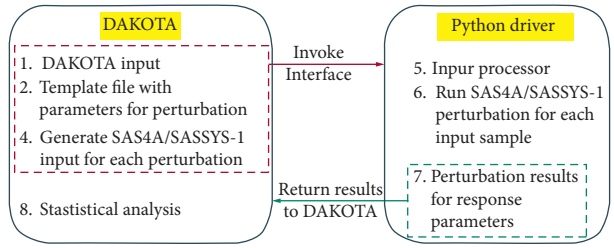

Figure 6: Schematic of the Python interface between DAKOTA and SAS4A/SASSYS-1.

Table 2: Eigenvalue comparison between serpent-2.0 and MCC-3.1/DIF3D.

	Serpent	MC^2-3.1	Δ pcm	% $\delta k/k$
Outer core	k_∞			
BOC	1.28194 ± 0.00014	1.28121	44.4	−0.05
EOC	1.25681 ± 0.00015	1.25813	−83.5	0.10
	Serpent	DIF3D		
2D core	k_∞			
BOC	1.17683 ± 0.00018	1.1688	583.8	0.66
EOC	1.15126 ± 0.00017	1.1437	574.2	0.91

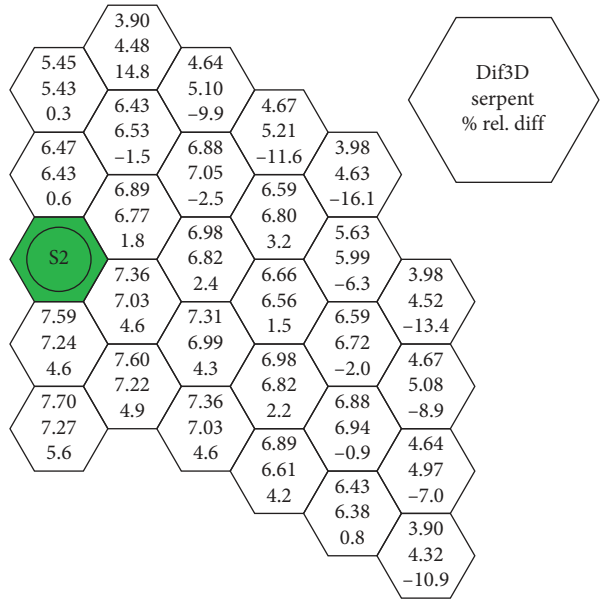

Figure 7: Power (MW) and relative difference (%) between serpent and Dif3D.

during UTOP transient. This provides an insight on the effect of uncertainties on core safety capabilities.

3.3. S&U Analysis of Lattice Level. Assemblywise S&U analysis is performed in Serpent as shown in Figures 10 and 11. The S&U profiles are generated for inner and outer core assemblies at BOC and EOC, respectively. Based on the sensitivity results, uncertainties relative to nuclide-reaction pairs are computed using the "Sandwich rule" described previously. The top five contributors to the uncertainty in k_{inf} at BOC and EOC for an inner core assembly are shown in Table 3.

The largest contribution to uncertainty in k_{inf} comes from heavy metals ^{235}U and ^{238}U. From Figures 10 and 11, the multiplication factor is noticeably sensitive to perturbations in the ^{235}U fission, ^{235}U ν, and ^{235}U capture cross section pairs. However, by considering reaction pair correlation coefficients from COMMARA-2.0 [7], the largest uncertainty contribution to the eigenvalue is from ^{235}U capture and ^{238}U inelastic reaction pairs.

On the 2D core level, Figure 12 shows large positive sensitivity of the eigenvalue to perturbations in ^{235}U ν cross section. At BOC, a positive perturbation in ^{235}U ν cross section leads to a positive response on reactivity. Similarly, negative sensitivity profile of ^{238}U-capture cross section is

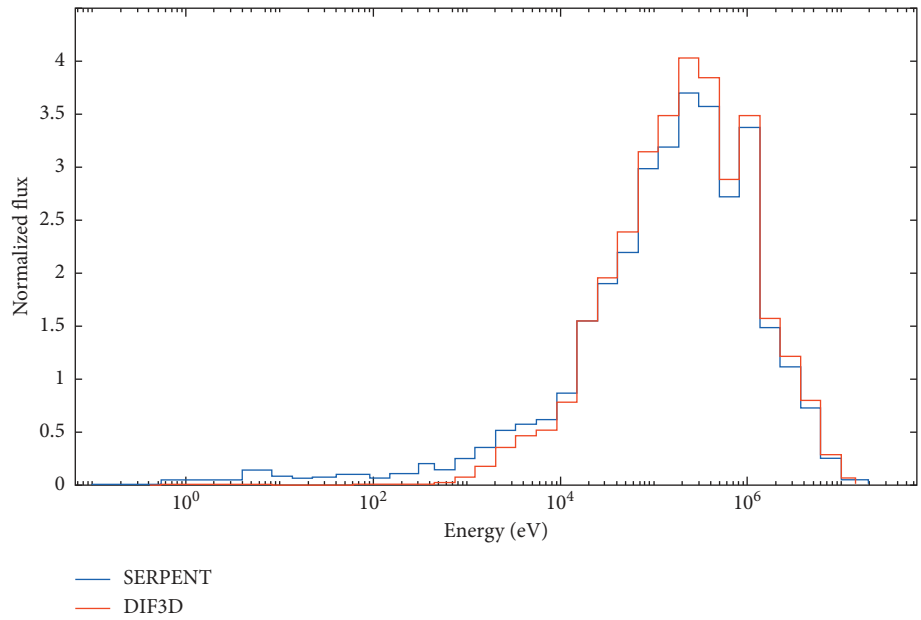

Figure 8: Normalized flux spectrum comparison for the central assembly (1, 1) between Dif3D and serpent.

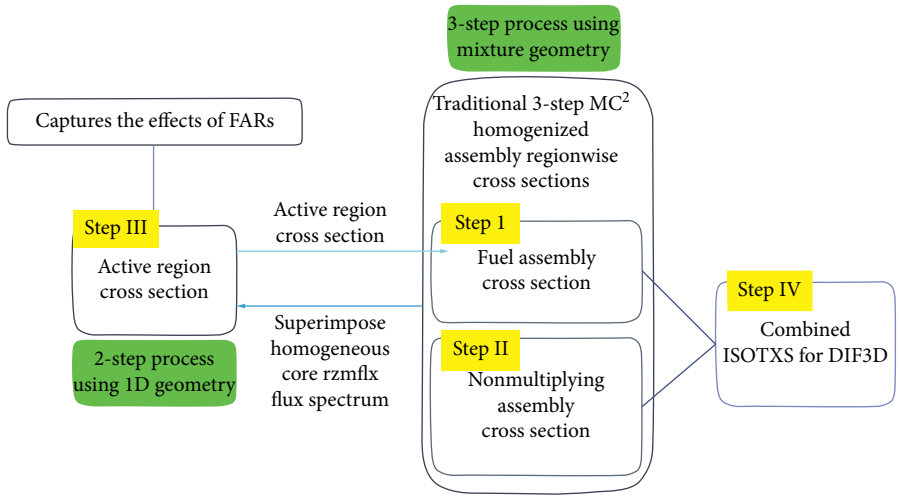

Figure 9: Improved cross section generation methodology for DLFR core.

evident since an increase of this reaction cross section type will lead to absorption of fast neutrons and decrease of the neutron population, introducing negative reactivity.

In addition, a substantial amount of uncertainty contribution from ^{235}U capture-^{235}U capture reaction pair is shown in Figure 13. This is not a surprising result considering the high enrichment in the core at BOC. The ^{238}U inelastic-^{238}U inelastic reaction pair provides the next largest contribution. Contribution from the top two nuclide-reaction pairs accounts for 85% of the uncertainty in k_{eff}. Furthermore, there is good comparison between the uncertainty profiles from Serpent and PERSENT based on the trends observed in Figure 13, although the values are not distinguishable in the lower energy range. This is likely due to the low flux in that region as shown in Figure 8. Comparisons between the remaining three nuclide-reaction pairs show a consistent trend between the two codes even with minor differences due to variations in the data points being obtained from two different codes.

3.4. S&U Analysis of Core Reactivity Feedback. Reactivity feedback coefficients are summarized in Table 4 to provide an understanding of the reactivity response to changes in temperature during reactor operation. The total uncertainty of each feedback coefficient from perturbations in nuclear data is also given in Table 4. Total uncertainty describes the total variance in the reactivity feedback parameter from perturbations in nuclear data.

The breakdown of the total uncertainty of neutronic feedback coefficients from Table 4 is provided in Figures 14 and 15 to show contributions from various reaction

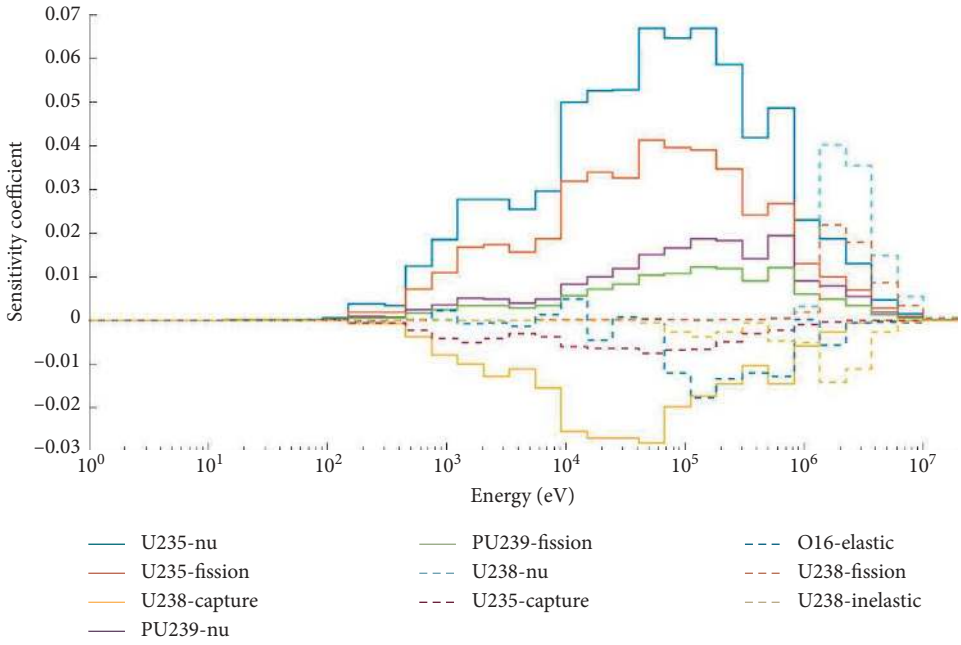

Figure 10: Sensitivity profile of k_{inf} for inner core assembly with BOC composition.

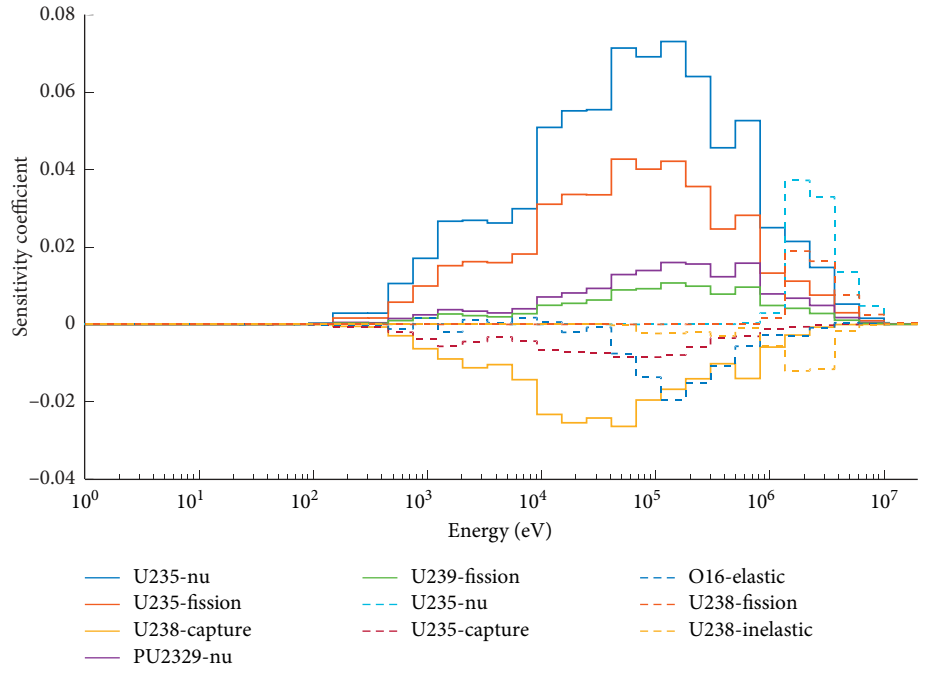

Figure 11: Sensitivity profile for outer core assembly with EOC composition.

channels. A large contribution is observed for Doppler reactivity and fuel density feedback coefficient (Figures 14(a) and 15(a), resp.) with BOC composition, where the majority of the uncertainty is seen to originate from ^{238}U inelastic scattering (Figure 14(a)) in high-energy range above 1 MeV. This can be associated with the significant sensitivity of the feedback coefficients to the perturbations in ^{238}U inelastic reaction cross section and strong reaction channel correlation in this energy range. For core radial expansion and structure feedback (Figures 14(b) and 15(b), resp.), ^{235}U fission and capture cross sections become significant in the epithermal range. Decreased structural density leads to reduced moderation, increased fission, and addition of uncertainty contribution from ^{235}U. Similarly, expansion of core pitch increases the coolant volume inside the reactor and adds negative reactivity.

Table 3: Relative contribution to uncertainty of k_{inf} for an inner assembly from serpent at BOC and EOC.

Rank	Uncertainty Contribution (%)			
	Nuclide/nuclide-reaction	BOC	Nuclide/nuclide-reaction	EOC
1	^{235}U $(n, \gamma)/^{235}$ U (n, γ)	65.8	^{235}U $(n, \gamma)/^{235}$U (n, γ)	54.7
2	^{238}U $(n, n')/^{238}$U (n, n')	19.1	^{238}U $(n, n')/^{238}$U (n, n')	27.9
3	^{238}U $(n, \gamma)/^{238}$U (n, γ)	5.11	^{238}U $(n, \gamma)/^{238}$U (n, γ)	5.86
4	^{235}U fission/^{235}U fission	1.74	^{235}U fission/^{235}U fission	1.81
5	^{56}Fe elastic/^{56}Fe elastic	1.73	^{16}O $(n, n)/^{16}$O (n, n)	1.52

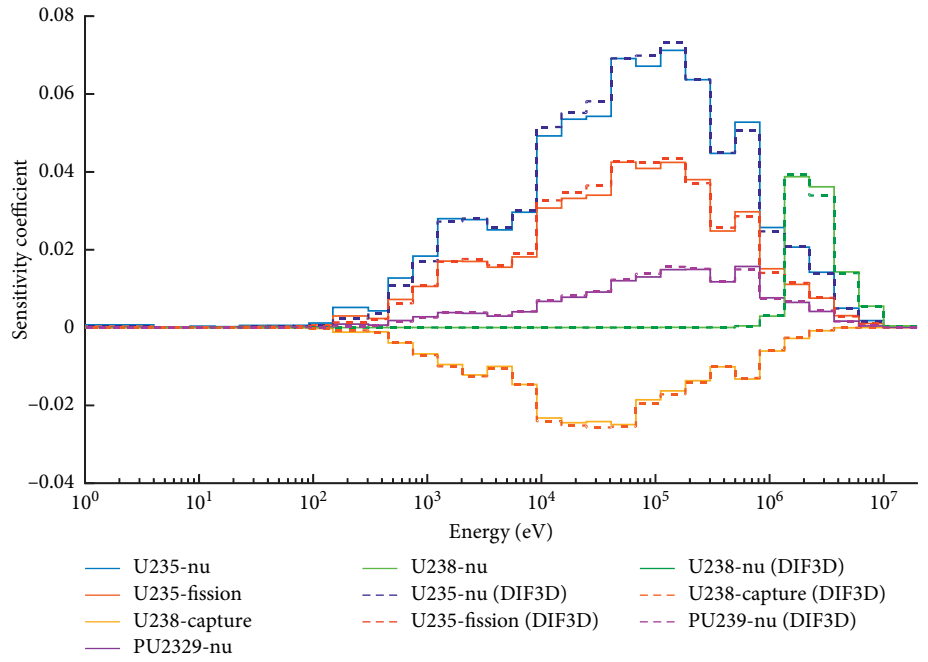

Figure 12: Sensitivity profiles for the top five cross sections to which k_{inf} is most sensitive at BOC (solid lines for serpent results, dashed lines for DIF3D results).

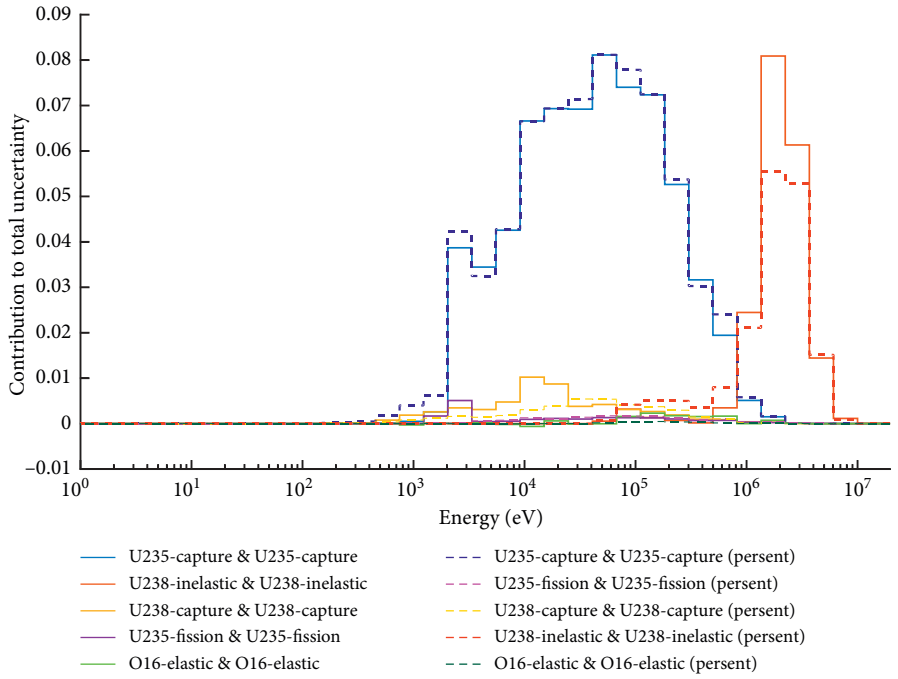

Figure 13: Uncertainty contribution from the main five isotopes at BOC (solid lines for serpent results, dashed lines for DIF3D results).

Table 4: Steady state neutronic reactivity feedback coefficients.

	$\Delta\rho$ doppler	$\Delta\rho$ fuel	$\Delta\rho$ coolant	$\Delta\rho$ structure	$\Delta\rho$ radial expansion
Coefficient (pcm/K)	−0.9240	−2.1450	−0.1720	+0.155	−0.8314
$\Delta\rho$ (pcm)	−713.51	−1423.98	−70.51	116.53	−851.31
Total uncertainty (%)	0.0102	0.1488	0.8398	0.0404	0.0637

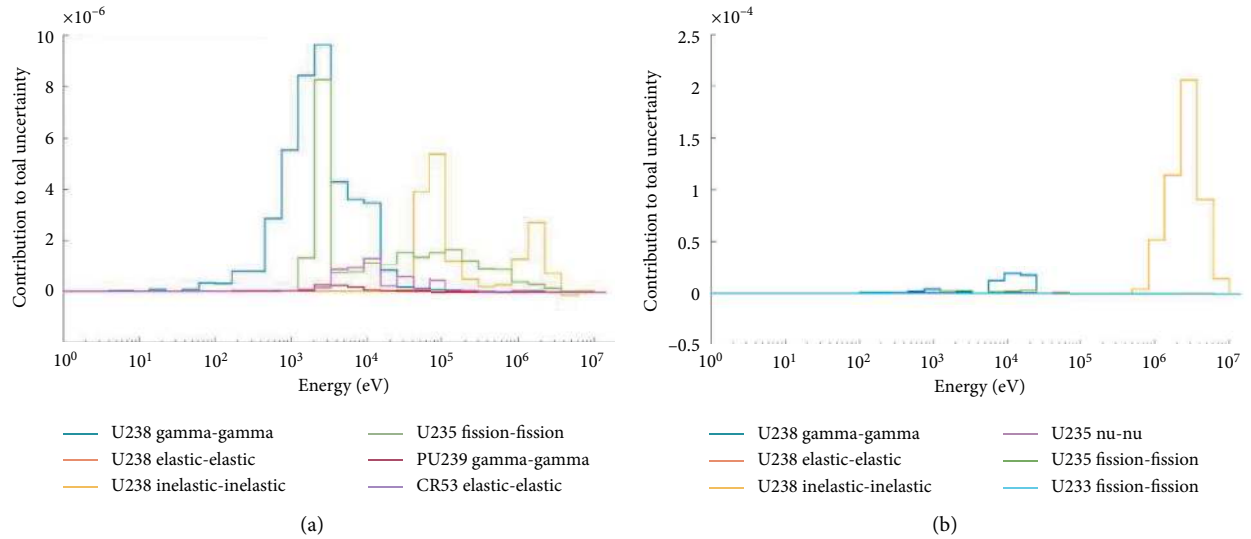

Figure 14: Contribution of major nuclide-reactions to uncertainties of (a) Doppler and (b) radial feedback coefficients.

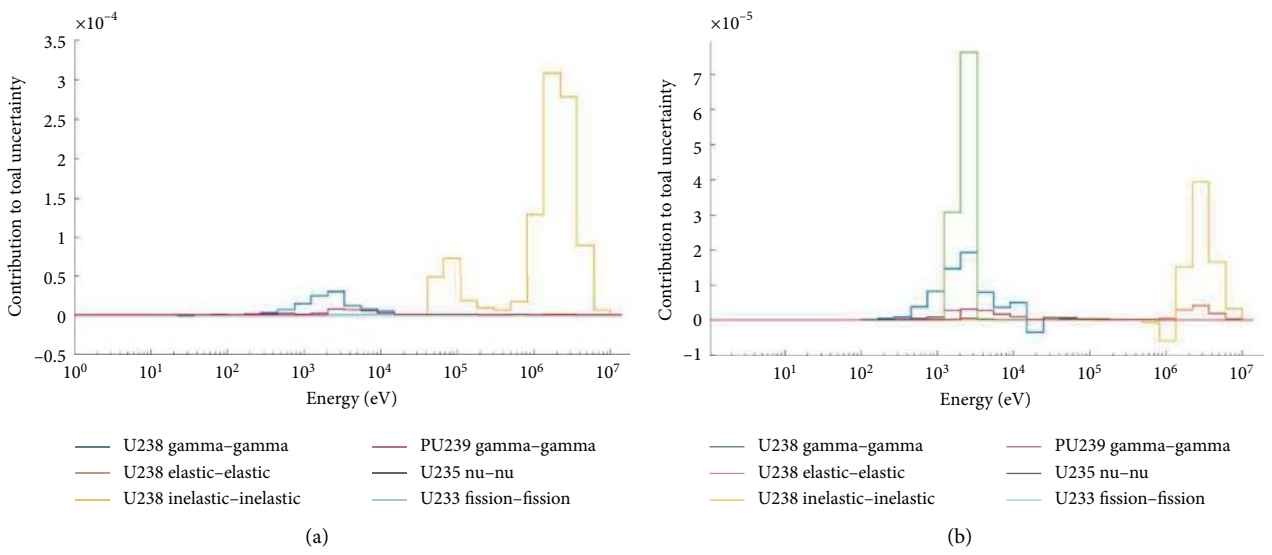

Figure 15: Contribution of major nuclide-reactions to uncertainties of (a) fuel and (b) structure feedback coefficients.

3.5. S&U Analysis of System Transient Simulations. After establishing steady state conditions, MiniSAS evaluates the temperature increase and associated reactivity feedback during an unprotected transient overpower (UTOP) accident. The transient is simulated with reactivity insertion of \$0.5 over 15 seconds to represent inadvertent rod withdrawal accident with reactivity ramp. No safety or control rods enter the core during this event. The pumps operate at full speed with heat transfer occurring via primary loop and emergency heat removal through DRACS. The remaining parameters conserve the nominal state conditions. Figure 16 shows the peak fuel, clad, and coolant temperatures as a function of transient time.

The reactivity ramp during transient increases the fuel temperature (Figure 16(a)) due to the increasing power, which in turn triggers a large negative Doppler reactivity countering the positive reactivity excursion (Figure 16(b)). Additional

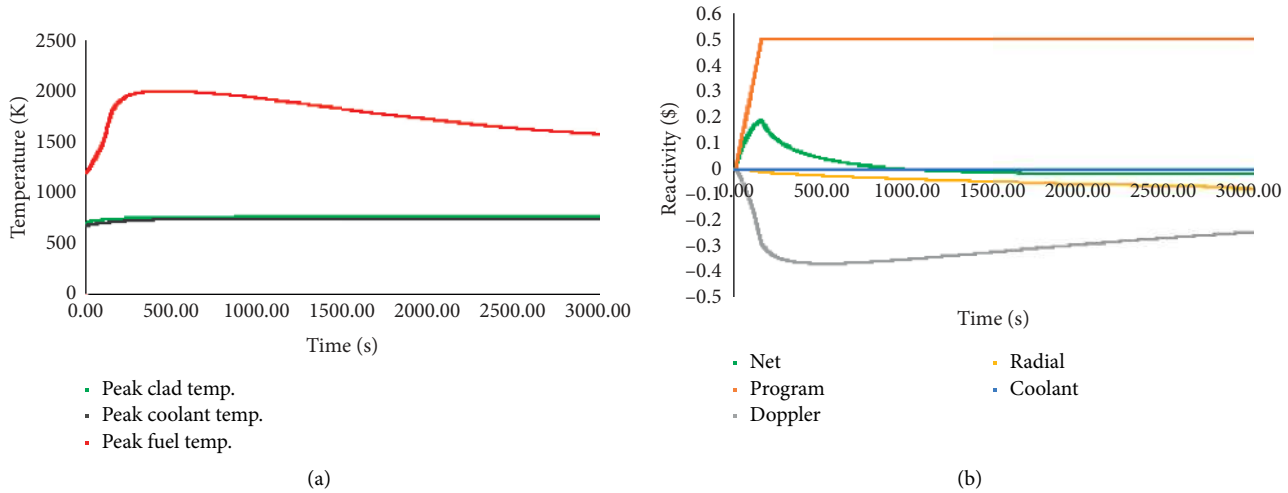

Figure 16: UTOP peak temperatures (a) and breakdown of the reactivity feedback by contribution (b).

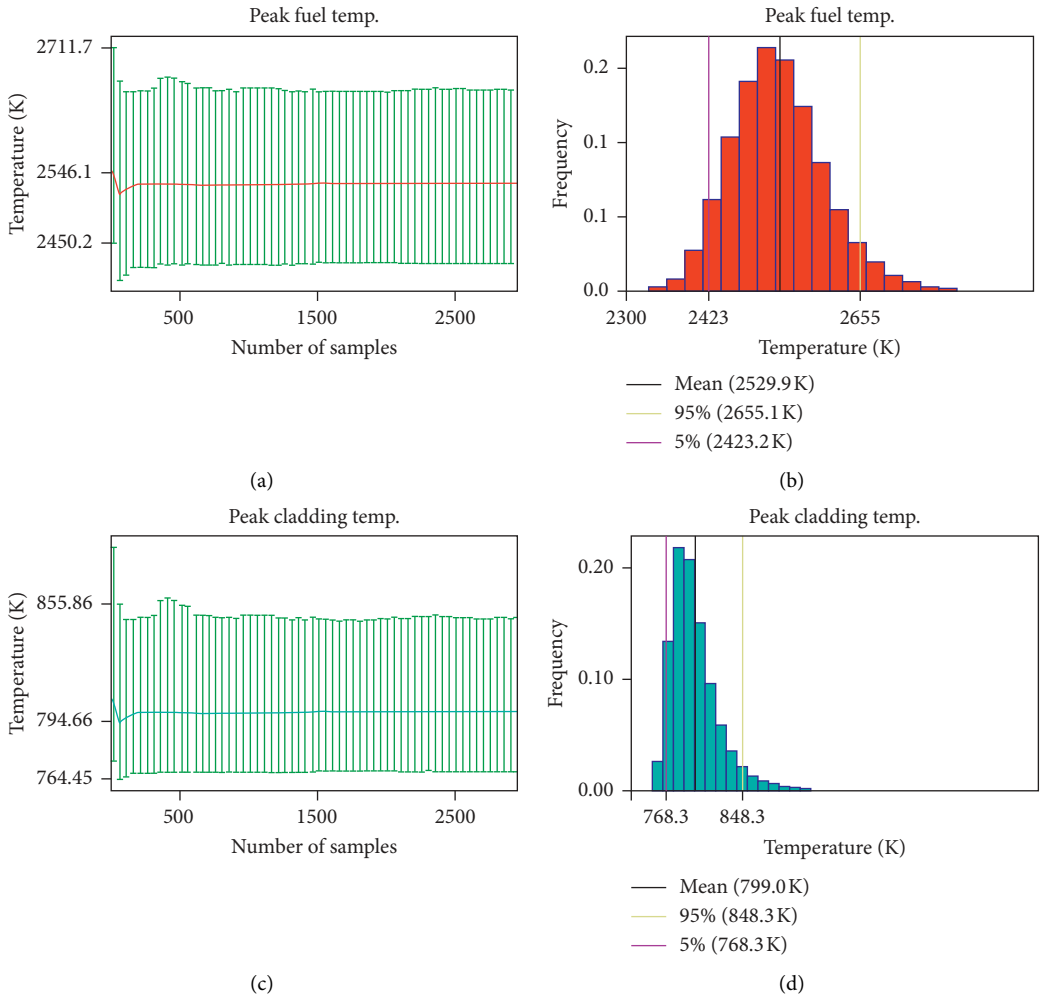

Figure 17: Sample convergence and spread of data for peak fuel and cladding temperatures during UTOP.

negative reactivity feedback from core flowering effect compensates for the remaining positive reactivity inserted during the transient. The fuel peak temperature remains well below the melting point of 3200 K for UO_2 fuel [15].

User-defined input uncertainties are propagated independently by perturbing input feedback coefficients on a normal distribution using LHS. Considering the preliminary nature of the SAS model, feedback parameters are currently

perturbed by 1% to set up a framework for UQ&P. This will be updated in future work.

An initial analysis is performed to obtain peak mean temperatures during transient. Due to the lack of substantial references for the DLFR, results are compared with a more mature LFR design, ALFRED, and its safety limits [26]. Figure 17 shows the peak fuel and cladding temperatures distribution for 3,000 samples analysed in DAKOTA with the 5%/95% interval bounds. The mean value for the DLFR peak fuel temperature is 2529.9 K, which is lower than the 3093.1 K observed for the ALFRED core during UTOP [26]. This is suspected due to different fuel types used in ALFRED (MOX) and the different reactivity insertion assumed in the safety analysis (0.7$ in 10 s) [26]. The mean peak clad temperature for the DLFR at 799.0 K is below the safety margin of 650°C (923.1 K) established in ALFRED [26] considering the creep rupture of stainless steel (used in both core designs). Lastly, both DLFR temperature values display large uncertainties of 70.0 K and 28.5 K for the peak fuel and clad temperatures, respectively, compared to similar analysis done on ABR1000 which shows 1.01°C and 0.84°C uncertainty in the two temperatures, respectively [19]. These large uncertainties for DLFR peak temperatures could be from the associated uncertainty of feedback coefficients (Table 4) which are being propagated independently without consideration of correlations between uncertainties. Therefore, further analysis is needed to investigate the magnitude of these uncertainties including correlated propagation of uncertainties. Sensitivity analysis of the peak fuel and clad temperatures to perturbation of these system model parameters will also be conducted to identify contributors of these uncertainties.

4. Conclusions and Future Work

In this paper, nuclear data input uncertainties in the DLFR core are studied using the Best Estimate Plus Uncertainty Methods. Primary modelling and UQ tools include the ANL fast reactor code suite ARC and Serpent-2.0. The core model is developed in Dif3D with cross sections generated by MCC-3.1 coupled with TWODANT. Serpent-2.0 is used to perform the lattice calculations and to verify ARC core parameters (eigenvalues, flux, and power profiles). On full core level, a modified cross section generation methodology is implemented in MCC-3.1 to improve the representation of the radial and axial heterogeneity in fuel assemblies. Preliminary results show a difference of 950 pcm in eigenvalues between conventional and improved methods. Further verification of the improved cross section method will be performed with Serpent and NEAMS Workbench/PyARC [27] in the future work.

In steady state, the uncertainties of the eigenvalue and feedback coefficients are quantified using perturbation theory by the PERSENT code with covariance matrix COMMARA-2.0. The multiplication factor shows the most sensitivity to perturbations in ^{235}U-fission cross section and ^{235}U ν and ^{238}U-capture cross section. This is followed by ^{239}Pu and ^{238}U-capture cross sections as the fuel experiences burnup. A statistical correlation coefficients matrix from COMMARA-2.0 determines the contribution of uncertainties from various nuclide-reaction pairs to identify the top contributing parameters. The ^{235}U capture-^{235}U capture and ^{238}U inelastic-^{238}U inelastic reaction pairs contribute the most to uncertainty at BOC. Propagation of these uncertainties through the reactor system will provide an insight on core safety capabilities.

The propagation of uncertainties requires standard deviations of reactivity feedback coefficients for five reactivity feedbacks, including the Doppler coefficient, radial expansion coefficient, and fuel/coolant/structure density worth. Significant uncertainty contributors of these coefficients are traced back to common nuclide-reaction pairs including ^{238}U inelastic and ^{238}U capture and ^{239}Pu capture cross sections. These uncertainties are propagated through an UTOP transient to evaluate their contribution on core safety performance. The system modelled in MiniSAS is adapted from the AB1000 model with necessary modifications. Latin Hypercube Sampling technique implemented within DAKOTA propagates uncorrelated uncertainties through the system. Large uncertainties in peak clad and fuel temperatures of 28.5 K and 70.0 K, respectively, are observed for the simulated UTOP. The sources of uncertainties in transient temperatures have not yet been identified. It is suspected that large contributions are originating from uncertainties of various feedback coefficients which are propagated independently without considering correlations between the uncertainties themselves. Furthermore, these uncertainties can be magnified from approximations in coolant properties and fuel description in MiniSAS.

In the future work, sensitivity analysis will be performed to determine the magnitude of sensitivity of peak fuel/clad temperatures to perturbations in various feedback coefficients. The overall UQ&P methodology will be expanded to include other sources of uncertainties (e.g., manufacturing and fuel performance uncertainties) through multiple transient scenarios such as unprotected loss of flow (ULOF). Additionally, the UQ&P method will be improved to account for correlations between uncertainties of various feedback coefficients. Lastly, for all future LFR safety analysis, the currently approximated LFR system model will be updated with a DLFR specific SAS model, recently obtained from WEC.

Data Availability

Specifications of the DLFR and ALFRED core design and performance can be found in [8, 26]. Cross section libraries were made available with the codes and COMMARA-2.0 library can be found through the OECD/NEA website. The authors are the end user of the reactor design and covariance data but do not have permissions to distribute it. The calculation results have been shown in the paper that the readers already have access to.

Disclosure

The research was performed as part of the author's doctoral research appointment at North Carolina State University.

Conflicts of Interest

The authors declare that there are no conflicts of interest regarding the publication of this paper.

References

[1] OECD Nuclear Energy Agency, *Handbook on Lead-bismuth Eutectic Alloy and Lead Properties, Materials Compatibility, Thermal-hydraulics and Technologies*, OECD Nuclear Energy Agency, Paris, France, 2015.

[2] F. D'Auria, C. Camargo, and O. Mazzantini, "The best estimate plus uncertainty (BEPU) approach in licensing of current nuclear reactors," *Nuclear Engineering and Design*, vol. 248, pp. 317–328, 2012.

[3] E. Alhassan, H. Sjöstrand, J. Duan et al., "Uncertainty analysis of lead cross sections on reactor safety for electra," in *Proceedings of the Joint International Conference on Supercomputing in Nuclear Applications*, Monte Carlo, France, June 2014.

[4] E. Alhassan, H. Sjöstrand, P. Helgesson et al., "Uncertainty and correlation analysis of lead nuclear data on reactor parameters for the European lead cooled training reactor," *Annals of Nuclear Energy*, vol. 75, pp. 26–37, 2015.

[5] M. Milosevic, "Effects of uncertainties in lead cross section data in Monte Carlo analysis of lead cooled and reflected reactors," in *Proceedings of the Conference on Mathematics & Computational Sciences (M&C)*, Monterey, CA, USA, 2007.

[6] R. C. Smith, *Uncertainty Quantification Theory Implementaion and Application*, Society of Indian Automobile Manufacturers, Raleigh, NC, USA, 2014.

[7] M. Herman, *AFCI-2.0 Neutron Cross Section Covariance Library*, Brookhaven National Laboratory, Upton, NY, USA, 2011.

[8] G. Grasso, *Demonstration Lead-cooled Fast Reactor*, Westinghouse Electric Company, Pittsburgh, PA, USA, 2016.

[9] B. J. Toppel, *Argonne Reactor Computation (ARC) System*, Argonne National Laboratory, Lemont, IL, USA, 1967.

[10] M. A. Smith, *MCC-3: Multigroup Cross-Section Generation Code for Fast Reactor Analysis*, Argonne National Laboratory, Lemont, IL, USA, 2013.

[11] R. Alcouffe, *User Guide for TWODANT: A Code Package for Two-Dimensional Diffusion Accelerated Neutral Particle Transport*, Los Alamos National Laboratory, Los Alamos, NM, USA, 1984.

[12] K. L. Derstine, *Dif3D: A Code Package to Solve One, Two, and Three Dimensional Finite Difference Dissuion Theory Problems*, Argonne National Laboratory, Lemont, IL, USA, 1984.

[13] J. Leppanen, M. Pusa, T. Viitanen, V. Valtavirta, and T. Kaltiaisenaho, "The serpent Monte Carlo code: status, development and applications," in *Proceedings of the Supercomputing In Nuclear Applications + Monte Carlo*, Monte Carlo, France, June 2014.

[14] A. Del Nevo, "Modelling and analysis of nuclear fuel pin behavior for innovative lead cooled FBR," 2014.

[15] S. G. Popov, *Thermophysical Properties of MOX and UO2 Fuels Including the Effects of Irradiation*, Oak Ridge National Laboratory, Knoxville, TN, USA, 2000.

[16] C. Lee, "Improved reactivity worth estimation of MCC-3/DIF3D in fast reactor analysis," in *Proceedings of the ANS Summer Meeting*, San Antonio, TX, USA, 2015.

[17] T. H. Fanning, *Status of the SAS4A/SASSYS-1 Safety Analysis Code*, Argonne National Laboratory, Lemont, IL, USA, 2017.

[18] T. H. Fanning, *SAS4A/SASSYS-1 Code Improvements for FY 2016*, Argonne National Laboratory, Lemont, IL, USA, 2016.

[19] N. Stauff, "Uncertainty quantification of ABR transient safety analysis," in *Proceedings of the Best Estimate Plus Uncertainty (BEPU)*, Lucca, Italy, 2018.

[20] G. Dan, "LFR design: safety, neutronics, thermal hydraulics, structural mehcanics, fuel, core and plant design," in *Handbook of Nuclear Engineering*, pp. 2821–2824, Springer, Berlin, Germany, 2010.

[21] N. Stauff, "Uncertainty quantification of ABR transient safety analysis-nuclear data uncertainties," in *Proceedigs of the Best Estimate Plus Uncertainty (BEPU)*, Lucca, Italy, 2018.

[22] M. A. Smith, *VARI3D & PERSENT: Perturbation and Sensitivity Analysis*, Argonne National Laboratory, Lemont, IL, USA, 2013.

[23] N. Stauff, *Private Communication*, Argonne National Laboratory, Lemont, IL, USA, 2019.

[24] M. Aufiero, A. Bidaud, M. Hursin et al., "A collision history-based approach to sensitivity/perturbation calculations in the continuous energy Monte Carlo code serpent," *Annals of Nuclear Energy*, vol. 85, pp. 245–258, 2015.

[25] B. M. Adams, "Dakota, a multilevel parallel object-oriented framework for design optimization, parameter estimation, uncertainty quantification, and sensitivity analysis: version 6.9 manual," 2018.

[26] G. Grasso, C. Petrovich, D. Mattioli et al., "The core design of alfred, a demonstrator for the European lead-cooled reactors," *Nuclear Engineering and Design*, vol. 278, pp. 287–301, 2014.

[27] N. Stauff, *Status of the NEAMS and ARC Neutronic Fast Reactortools Integration to the NEAMS Workbench*, Argonne National Laboratory, Lemont, IL, USA, 2019.